

Fast High-Dimensional Kernel Filtering

Pravin Nair, *Student Member, IEEE* and Kunal N. Chaudhury, *Senior Member, IEEE*

Abstract—The bilateral and nonlocal means filters are instances of kernel-based filters that are popularly used in image processing. It was recently shown that fast and accurate bilateral filtering of grayscale images can be performed using a low-rank approximation of the kernel matrix. More specifically, based on the eigendecomposition of the kernel matrix, the overall filtering was approximated using spatial convolutions, for which efficient algorithms are available. Unfortunately, this technique cannot be scaled to high-dimensional data such as color and hyperspectral images. This is simply because one needs to compute/store a large matrix and perform its eigendecomposition in this case. We show how this problem can be solved using the Nyström method, which is generally used for approximating the eigendecomposition of large matrices. The resulting algorithm can also be used for nonlocal means filtering. We demonstrate the effectiveness of our proposal for bilateral and nonlocal means filtering of color and hyperspectral images. In particular, our method is shown to be competitive with state-of-the-art fast algorithms, and moreover it comes with a theoretical guarantee on the approximation error.

Index Terms—Kernel Filter, Nyström Method, Approximation, Fast Algorithm, Error Bound.

I. INTRODUCTION

The bilateral and nonlocal means filters [1], [2] are widely used for edge-preserving smoothing and denoising of images [3], [4]. These are instances of kernel filters, where the similarity (affinity) between pixels is measured using a symmetric kernel. We refer the reader to [4] for an excellent review of kernel filters. While they have proven to be useful in practice, a flip side of kernel filtering, including bilateral filtering (BLF) and nonlocal means (NLM), is their computational complexity [3]. Nevertheless, several fast algorithms have been proposed, e.g. [5]–[26], which can speed up BLF and NLM, without compromising their filtering quality. See [11], [21], [26] for a survey of these algorithms. Unfortunately, most algorithms only work with grayscale images, and cannot be extended to color, multispectral, and hyperspectral images.

Algorithms for fast BLF of color images have been proposed in [12], [21], [27]–[29]. However, to the best of our knowledge, these methods have not been extended for multispectral and hyperspectral images. Fast algorithms for generic high-dimensional BLF and NLM have been proposed in [18]–[20], [30]. A common feature of these algorithms is that they use data clustering or tessellation in high-dimensions. The state-of-the-art fast algorithms for color BLF are [19], [21], and for color NLM is [20].

More recently, it was shown in [15], [17] that fast BLF of grayscale images can be performed using the partial eigendecomposition of the kernel matrix. In fact, the interpretation of BLF (and NLM) as kernel filters goes back to [31]–[33]. While the Nyström method has widely been used in machine learning [34]–[36], it appears that [31] is the first to apply this

for image filtering. Note that, unlike [15], [17], the spatial and range kernel are treated as a single kernel in [31]–[33].

The differences between our and related approaches are:

- As explained in detail in §II, it is difficult to scale [15], [17] for filtering high-dimensional (even color) images, since one needs to populate a huge kernel matrix and compute its eigendecomposition. We propose to use the Nyström method to solve this problem. As a result, we are able to perform BLF and NLM of color and hyperspectral images.

- The first difference with [31]–[33] is that we use clustering instead of uniform sampling for the Nyström approximation. A significant improvement in filtering accuracy is achieved as a result. The other difference is that if a spatial kernel has to be incorporated in [31]–[33], then the Nyström approximation needs to be performed in the spatio-range space. However, we handle the spatial and range components differently—fast convolutions are used for the spatial component and Nyström approximation is used for the range component. As a result, we require lesser samples for the Nyström approximation.

- In [28], [29], clustering is used to compute “intermediate” images, which are interpolated to get the final output. On the other hand, clustering is used in our method just to obtain the “landmark points” for the Nyström approximation.

- Compared to [18]–[21], our algorithm is conceptually simple and easy to implement. Moreover, we are able to derive a bound on the filtering error incurred by the approximation. Such a guarantee is not offered by [18]–[21].

The rest of the paper is organized as follows. In §II, we introduce the notion of kernel filtering, and explain the core problem in relation to the spectral approximations in [15], [17]. We use the Nyström method in §III to overcome this problem. Numerical results are reported in §IV and we conclude in §V.

II. BACKGROUND

We begin by formulating BLF and NLM as kernel filters [4]. Suppose the input image is $\mathbf{f} : \Omega \rightarrow [0, R]^n$, where $\Omega \subset \mathbb{Z}^d$ is the spatial domain, $[0, R]^n$ is the range space, and d (resp. n) is the dimension of the domain (resp. range). Let $\mathbf{p} : \Omega \rightarrow [0, R]^\rho$ be the *guide* image, which is used to control the filtering. For standard BLF, \mathbf{f} and \mathbf{p} are identical, and $n = \rho = 1$ and 3 for grayscale and color images. However, \mathbf{f} and \mathbf{p} (also n and ρ) can be different for joint BLF [3]. For NLM, ρ is generally larger than n , where ρ is the number of pixels in a *patch* [2]. Let $\kappa : \mathbb{R}^\rho \times \mathbb{R}^\rho \rightarrow \mathbb{R}$ be the *range* kernel. The filtered output $\mathbf{g} : \Omega \rightarrow [0, R]^n$ is given by

$$\mathbf{g}(\mathbf{x}) = \frac{\sum_{\mathbf{y} \in W_{\mathbf{x}}} \omega(\mathbf{x} - \mathbf{y}) \kappa(\mathbf{p}(\mathbf{x}), \mathbf{p}(\mathbf{y})) \mathbf{f}(\mathbf{y})}{\sum_{\mathbf{y} \in W_{\mathbf{x}}} \omega(\mathbf{x} - \mathbf{y}) \kappa(\mathbf{p}(\mathbf{x}), \mathbf{p}(\mathbf{y}))}, \quad (1)$$

where $W_{\mathbf{x}}$ is a square window around $\mathbf{x} \in \Omega$ consisting of $(2S+1)^d$ pixels, with S being the window radius. The *spatial*

kernel $\omega : \mathbb{Z}^d \rightarrow \mathbb{R}$ controls the weighting of the neighboring pixels involved in the averaging. At this point, we just assume that κ is symmetric, i.e., $\kappa(\mathbf{t}, \mathbf{s}) = \kappa(\mathbf{s}, \mathbf{t})$ for $\mathbf{t}, \mathbf{s} \in \mathbb{R}^\rho$. For example, $\kappa(\mathbf{t}, \mathbf{s}) = \exp(-\theta \|\mathbf{s} - \mathbf{t}\|^2)$, $\theta > 0$, for standard BLF and NLM, where $\|\cdot\|$ is the Euclidean norm.

It was shown in [15], [17] that the non-linear operations in (1) can be computed using convolutions by approximating κ . For convenience, we will describe this using our notations. Let the actual range of \mathbf{p} be

$$\mathfrak{R} = \{\mathbf{p}(\mathbf{x}) : \mathbf{x} \in \Omega\}. \quad (2)$$

We emphasize that \mathfrak{R} is a list and not a set, i.e., we allow repetition of elements in \mathfrak{R} . In particular, let $\mathfrak{R} = \{\mathbf{r}_1, \mathbf{r}_2, \dots, \mathbf{r}_m\}$ be some ordering of the elements in \mathfrak{R} , where m is the number of elements. This means that, given $\ell \in [1, m]$, $\mathbf{r}_\ell = \mathbf{p}(\mathbf{x})$ for some $\mathbf{x} \in \Omega$. We track this correspondence using the *index map* $\iota : \Omega \rightarrow [1, m]$, where

$$\iota(\mathbf{x}) = \ell \quad \text{if } \mathbf{r}_\ell = \mathbf{p}(\mathbf{x}). \quad (3)$$

We next define the kernel matrix $\mathbf{K} \in \mathbb{R}^{m \times m}$ given by

$$\mathbf{K}(i, j) = \kappa(\mathbf{r}_i, \mathbf{r}_j). \quad (4)$$

In terms of (4), we can write (1) as

$$\mathbf{g}(\mathbf{x}) = \frac{\sum_{\mathbf{y} \in W_{\mathbf{x}}} \omega(\mathbf{x} - \mathbf{y}) \mathbf{K}(\iota(\mathbf{x}), \iota(\mathbf{y})) \mathbf{f}(\mathbf{y})}{\sum_{\mathbf{y} \in W_{\mathbf{x}}} \omega(\mathbf{x} - \mathbf{y}) \mathbf{K}(\iota(\mathbf{x}), \iota(\mathbf{y}))} \quad (5)$$

It is clear from (4) that \mathbf{K} is symmetric. In particular, let the eigendecomposition of \mathbf{K} be

$$\mathbf{K} = \sum_{k=1}^m \lambda_k \mathbf{u}_k \mathbf{u}_k^\top, \quad (6)$$

where $\lambda_1, \dots, \lambda_m \in \mathbb{R}$ are its eigenvalues, and $\mathbf{u}_1, \dots, \mathbf{u}_m \in \mathbb{R}^m$ are the corresponding eigenvectors. Substituting (6) in (5), we can write its numerator as

$$\sum_{\mathbf{y} \in W_{\mathbf{x}}} \omega(\mathbf{x} - \mathbf{y}) \left\{ \sum_{k=1}^m \lambda_k \mathbf{u}_k(\iota(\mathbf{x})) \mathbf{u}_k(\iota(\mathbf{y})) \right\} \mathbf{f}(\mathbf{y}).$$

On switching the sums, this becomes

$$\sum_{k=1}^m \lambda_k \mathbf{u}_k(\iota(\mathbf{x})) (\omega * \mathbf{h}_k)(\mathbf{x}), \quad (7)$$

where $\omega * \mathbf{h}_k$ denotes the convolution of the image $\mathbf{h}_k(\mathbf{x}) = \mathbf{u}_k(\iota(\mathbf{x})) \mathbf{f}(\mathbf{x})$ with ω . An identical argument applies for the denominator. In summary, we can compute (5) using convolutions, for which several efficient algorithms are available [37], [38]. Moreover, by considering just the largest eigenvalues, fast and accurate approximations can be obtained [15], [17].

Unfortunately, computing the full kernel and its eigendecomposition becomes prohibitively expensive when ρ is large. Just as an example, consider an 8-bit color image for which $R = 255$ and $\rho = 3$. Even if we assume that m is just 10% of the maximum range cardinality ($= 256^3$), we will still need to populate a 3 million \times 3 million matrix, and compute its eigenvalues. The situation is worse for hyperspectral images, where ρ is of the order of tens, or even hundreds.

III. PROPOSED METHOD

Originally, the Nyström method was used for approximating the solution of functional eigenvalue problems [39], [40]. The method has found useful applications in machine learning and computer vision for approximating the eigendecomposition of large matrices [31], [34], [35]. In the present context, the goal is to approximate (6) using a decomposition of the form

$$\widehat{\mathbf{K}} = \sum_{k=1}^{m_0} \alpha_k \mathbf{v}_k \mathbf{v}_k^\top, \quad (8)$$

where $\alpha_k \in \mathbb{R}$ and $\mathbf{v}_k \in \mathbb{R}^m$. Clearly, the rank of $\widehat{\mathbf{K}}$ is at most m_0 . Thus, for small m_0 , $\widehat{\mathbf{K}}$ is a low-rank approximation of \mathbf{K} . A large m_0 results in a better approximation, but at higher computational cost. In practice, a good tradeoff is required.

The original kernel \mathbf{K} is defined on \mathfrak{R} . In the Nyström method [39], [40], we first construct a smaller kernel \mathbf{A} , compute its eigendecomposition, and then “extrapolate” the eigenvectors of \mathbf{A} to approximate those of \mathbf{K} . More precisely, we pick few *landmarks* points from \mathfrak{R} , say, $\mathfrak{R}_0 = \{\boldsymbol{\mu}_1, \dots, \boldsymbol{\mu}_{m_0}\}$, and define a kernel $\mathbf{A} \in \mathbb{R}^{m_0 \times m_0}$ on \mathfrak{R}_0 :

$$\mathbf{A}(i, j) = \kappa(\boldsymbol{\mu}_i, \boldsymbol{\mu}_j) \quad (i, j \in [1, m_0]). \quad (9)$$

Clearly, \mathbf{A} is symmetric, and its size is much smaller than \mathbf{K} . Thus, we can efficiently compute its eigendecomposition:

$$\mathbf{A} = \sum_{k=1}^{m_0} \alpha_k \mathbf{w}_k \mathbf{w}_k^\top, \quad (10)$$

where $\alpha_k \in \mathbb{R}$ and $\mathbf{w}_k \in \mathbb{R}^{m_0}$. We next construct $\mathbf{B} \in \mathbb{R}^{m_0 \times m}$ on $\mathfrak{R}_0 \times \mathfrak{R}$ given by

$$\mathbf{B}(i, j) = \kappa(\boldsymbol{\mu}_i, \mathbf{r}_j), \quad (11)$$

where $i \in [1, m_0]$ and $j \in [1, m]$. This captures the kernel values between the points in \mathfrak{R} and the landmark points. This matrix is used to extrapolate \mathbf{w}_k as follows:

$$\mathbf{v}_k = \frac{1}{\alpha_k} \mathbf{B}^\top \mathbf{w}_k \quad (k \in [1, m_0]). \quad (12)$$

This completes the specification of α_k and \mathbf{v}_k in (8). We refer the reader to [35] for the intuition behind the approximation. The effective speedup of replacing (6) by (8) is $\mathcal{O}(m/m_0)^3$. This is because the complexity of eigendecomposition of a $k \times k$ matrix is $\mathcal{O}(k^3)$ [41]. In particular, the speedup is significant since $m_0 \ll m$. As will be evident shortly, we just need to compute (α_k) and (\mathbf{v}_k) ; we will not use $\widehat{\mathbf{K}}$ explicitly.

Following [36], we select the landmark points by clustering \mathfrak{R} . More specifically, we partition \mathfrak{R} into m_0 disjoint sets using k -means clustering, and take the centroids to be the landmarks. Note that, though \mathfrak{R}_0 is not guaranteed to be a subset of \mathfrak{R} , we can still apply the above approximation.

It was shown in [36] that the *kernel error* can be bounded by the *quantization error*. More specifically, let $\|\mathbf{K} - \widehat{\mathbf{K}}\|_F$ be the kernel error ($\|\cdot\|_F$ is the Frobenius norm), and let

$$e = \sum_{i=1}^m \|\mathbf{r}_i - \boldsymbol{\mu}_{c(i)}\|^2$$

be the quantization error, where $c(i)$ is the minimizer of $\|\mathbf{r}_i - \boldsymbol{\mu}_j\|$ over $j \in [1, m_0]$. Then the following bound holds [36].

Proposition 1: Suppose there exists some $L > 0$ such that, for $\mathbf{w}, \mathbf{x}, \mathbf{y}, \mathbf{z} \in \mathfrak{R}$,

$$(\kappa(\mathbf{x}, \mathbf{y}) - \kappa(\mathbf{w}, \mathbf{z}))^2 \leq L(\|\mathbf{x} - \mathbf{w}\|^2 + \|\mathbf{y} - \mathbf{z}\|^2).$$

Then the approximation error can be bounded as

$$\|\mathbf{K} - \widehat{\mathbf{K}}\|_{\text{F}} \leq c_1\sqrt{e} + c_2e, \quad (13)$$

where the positive constants c_1 and c_2 do not depend on e . In particular, (13) holds when κ is a Gaussian.

Proposition 1 suggests that we can reduce the kernel error by making e small. However, e measures how well Θ is represented by the landmark points. Following this observation, k -means clustering was used in [36] for determining the landmarks. It was empirically shown in [36] that clustering indeed results in smaller error over uniform sampling [31], [35]. We will see that this is also true for our algorithm.

We arrive at a fast algorithm by replacing \mathbf{K} by $\widehat{\mathbf{K}}$. It is clear from (7) that the resulting approximation is given by

$$\hat{\mathbf{g}}(\mathbf{x}) = \frac{1}{\hat{\eta}(\mathbf{x})} \sum_{k=1}^{m_0} \alpha_k \mathbf{v}_k(\iota(\mathbf{x})) (\omega * \mathbf{h}_k)(\mathbf{x}), \quad (14)$$

$$\hat{\eta}(\mathbf{x}) = \sum_{k=1}^{m_0} \alpha_k \mathbf{v}_k(\iota(\mathbf{x})) (\omega * d_k)(\mathbf{x}), \quad (15)$$

where $d_k : \Omega \rightarrow \mathbb{R}$ and $\mathbf{h}_k : \Omega \rightarrow \mathbb{R}^n$ are defined as $d_k(\mathbf{x}) = \mathbf{v}_k(\iota(\mathbf{x}))$ and $\mathbf{h}_k(\mathbf{x}) = d_k(\mathbf{x})\mathbf{f}(\mathbf{x})$.

The computation of (14) and (15) involves $(n+1)m_0$ convolutions, since for each $k \in [1, m_0]$, there are n convolutions in (14) and one in (15). The main point is that we have been able to express the non-linear kernel filter using convolutions, for which efficient algorithms are available. In particular, (14) and (15) can be performed using $\mathcal{O}(1)$ operations (w.r.t. the size of the spatial kernel), when ω is a box or Gaussian [37], [38], [42]. The overall algorithm is described in Algorithm 1 (source code in [43]), where the symbols \oplus , \otimes and \oslash are used to denote pixelwise addition, multiplication, and division. The complexity of k -means clustering and the eigendecomposition of \mathbf{A} are $\mathcal{O}(|\Omega|m_0\rho)$ [44] and $\mathcal{O}(m_0^3)$ [41]. On the other hand, the complexity of the convolutions in (14) and (15) is $\mathcal{O}(|\Omega|m_0(n+\rho))$, where $|\Omega|$ is the number of pixels. Since the complexity of the brute-force implementation is $\mathcal{O}(|\Omega|(2S+1)^d(n+\rho))$ [3], and convolutions are the dominant operations in our algorithm, we obtain an effective speedup of $(2S+1)^d/m_0$. This is significant as S is typically large [3].

We now comment on the filtering accuracy, namely, how well is (1) approximated by (14). Intuitively, we expect the approximation to be accurate if $\widehat{\mathbf{K}} \approx \mathbf{K}$. In fact, since the difference $\|\mathbf{K} - \widehat{\mathbf{K}}\|_{\text{F}}$ is controlled by the quantization error (Proposition 1), we have the following result.

Theorem 2: Suppose ω and κ are positive, and κ satisfies the property in Proposition 1. Then

$$\|\hat{\mathbf{g}} - \mathbf{g}\|_{\infty} = \max_{\mathbf{x} \in \Omega} \|\hat{\mathbf{g}}(\mathbf{x}) - \mathbf{g}(\mathbf{x})\| \leq C_1\sqrt{e} + C_2e, \quad (16)$$

where $C_1, C_2 > 0$ do not depend on e .

The main steps of the derivation are given in the supplement. Theorem 2 is true for BLF and NLM, where κ is a Gaussian. A practical implication of this result is that the filtering accuracy

Algorithm 1: Fast Kernel Filtering.

Input: $\mathbf{f} : \Omega \rightarrow \mathbb{R}^n$ and $\mathbf{p} : \Omega \rightarrow \mathbb{R}^\rho$, kernels ω and κ ;

Parameter: Number of landmarks m_0 ;

Output: Approximation in (14);

Form \mathfrak{R} in (2) and index map ι in (3);

$\{\mu_k\} \leftarrow$ partition \mathfrak{R} into m_0 clusters using k -means;

Construct \mathbf{A} and \mathbf{B} in (9) and (11) using κ and \mathbf{p} ;

Compute the eigendecomposition of \mathbf{A} in (10);

Initialize $\zeta : \Omega \rightarrow \mathbb{R}^n$ and $\eta : \Omega \rightarrow \mathbb{R}$ with zeros;

for $k = 1, \dots, m_0$ **do**

$\mathbf{v}_k = (1/\alpha_k)\mathbf{B}^\top \mathbf{w}_k$;

for $\mathbf{x} \in \Omega$ **do**

$d_k(\mathbf{x}) = \mathbf{v}_k(\iota(\mathbf{x}))$;

$\mathbf{h}_k(\mathbf{x}) = d_k(\mathbf{x})\mathbf{f}(\mathbf{x})$;

end

$\zeta \leftarrow \zeta \oplus (\alpha_k \cdot d_k \otimes (\omega * \mathbf{h}_k))$;

$\eta \leftarrow \eta \oplus (\alpha_k \cdot d_k \otimes (\omega * d_k))$;

end

$\hat{\mathbf{g}} \leftarrow \zeta \oslash \eta$.

is guaranteed to increase with m_0 (Figure 4 in the supplement). Deriving a similar bound is difficult for [18]–[21].

IV. RESULTS

We demonstrate the effectiveness of our algorithm for BLF and NLM of high-dimensional images by comparing it with state-of-the-art algorithms. Instead of standard NLM [2], we have used PCA-NLM [45], where the denoising performance of the former is improved by applying PCA on the collection of patches. As for the dataset, we have used the color images from [46] and the hyperspectral images from [47]. Experiments were performed using Matlab on a 3.4 GHz quad-core machine with 32 GB memory. The spatial kernel ω for BLF is a Gaussian (covariance $\sigma^2\mathbf{I}$ and $S = 3\sigma$), while it is a box in PCA-NLM. The range kernel κ is Gaussian (covariance $\theta^2\mathbf{I}$) for both BLF and PCA-NLM. We have used the fast $\mathcal{O}(1)$ algorithm in [37] when ω is a Gaussian, and the Matlab routine “imfilter” when ω is a box. Note that we can also use other fast Gaussian filters [38], [42] if higher accuracy is desired.

Color BLF. The state-of-the-art fast algorithms for color BLF are Adaptive Manifolds (AM) [20], Permutohedral Lattice (PL) [19], and Global Color Sparseness (GCS) [21]. We have compared with them in Figure 2. The number of manifolds is set automatically in AM, whereas we have used 15 clusters in GCS and for the Nyström approximation. Following [20], [21], we used PSNR to measure the error between the brute-force and fast implementations. In Figure 2, notice that while our PSNR marginally exceeds that of GCS, it is however much better than PL and AM. Also notice the significant acceleration over the brute-force implementation obtained using our algorithm. We have also provided a table comparing the different methods on the Kodak dataset [46] in the supplement. The table shows that our method is better than GCS and PL when $\theta > 40$. As claimed in the introduction, we can see from the table that clustering provides a significant boost in filtering accuracy (10-20 dB) over uniform sampling.



Fig. 1. Gaussian denoising (noise level 25/255) of a color image using (b) PCA-NLM, its fast approximations (c) and (d), and (e) BM3D. The respective (Timing (sec), PSNR (dB), SSIM) is shown in the caption.

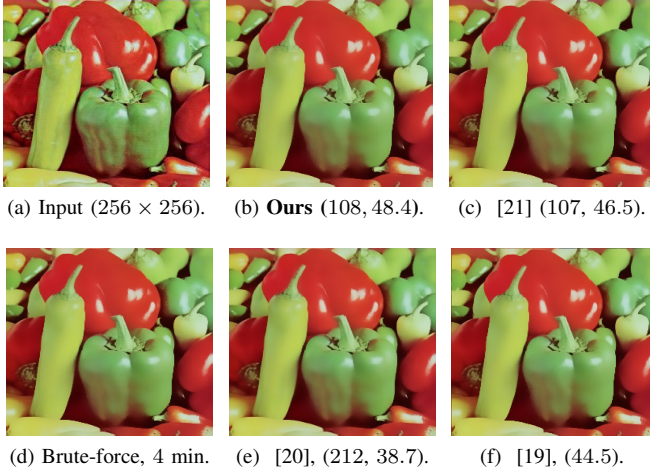


Fig. 2. Visual comparison for fast BLF at $\sigma = 5$, $\theta = 50$, and $|\Omega_0| = (6\sigma+1)^2$. The (timing, PSNR) are mentioned, where timing is in milliseconds and PSNR is in dB. Timing is not mentioned for [19] which is implemented in C++. The breakup of timing for the proposed method is as follows: clustering (11 ms), eigendecomposition (1 ms), and convolutions (96 ms). Note that the overall timing is dominated by the convolutions.

Color NLM. AM is the state-of-the-art fast algorithm for color NLM (and PCA-NLM). In NLM, $\rho = 3(2r+1)^2$, where r is the patch radius [2]. On the other hand, ρ is reduced to a smaller value in PCA-NLM using PCA. Following [45], we set θ to be three times the noise level for all experiments. Denoising results are shown in Figure 1, where $S = 10$ and $r = 3$. For (b), (c), and (d), PCA was used to reduce the range dimension from 3×7^2 to 25. We used 31 clusters (resp. manifolds) for the Nyström approximation (resp. AM). Following [50], we measured the denoising performance using PSNR and SSIM (between the clean and denoised images). Note that we are superior to AM both in terms of accuracy and timing. Importantly, our PSNR is close to PCA-NLM (the method being approximated), but we are about $160\times$ faster. In comparison with BM3D [51], our PSNR is 3 dB less. However, our timing is about half that of BM3D, since our complexity is much less than that of BM3D. Additional visual comparisons and accuracy analysis is provided in the supplement.

Hyperspectral BLF. Finally, we present a denoising result for a hyperspectral image of size $(610 \times 340) \times 103$ bands using BLF ($\sigma = 3, \theta = 100$). We have also compared with state-of-the-art methods for hyperspectral denoising [48], [49], whose parameters have been tuned accordingly. The results are shown in Figure 3. We have used $m_0 = 32$ landmarks for the

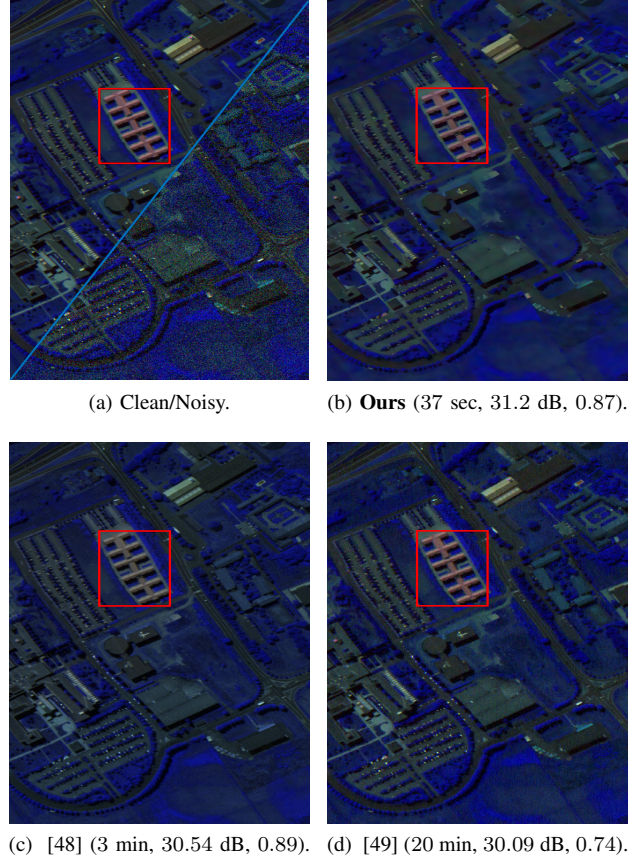


Fig. 3. Hyperspectral denoising of a natural image corrupted with Gaussian noise of level 25/255. (Timing, PSNR, SSIM) are shown for all methods.

Nyström approximation. As a standard practice, the PSNR and SSIM values are averaged over the spectral bands. Notice that our method can restore details better, which results in higher PSNR/SSIM values. In particular, the color is not satisfactorily restored in [48] and grains can be seen in [49]. Being a one-shot method, we are much faster than [48], [49].

V. CONCLUSION

We showed that fast bilateral and nonlocal means filtering of high-dimensional images can be performed using the Nyström approximation. The proposed algorithm can significantly accelerate the brute-force implementation of these filters, without compromising the visual quality. In particular, our algorithm is often competitive with state-of-the-art fast algorithms, and comes with provable guarantee on the filtering accuracy.

REFERENCES

- [1] C. Tomasi and R. Manduchi, "Bilateral filtering for gray and color images," *Proc. IEEE International Conference on Computer Vision*, pp. 839–846, 1998.
- [2] J. Buades, B. Coll, and J.-M. Morel, "A non-local algorithm for image denoising," *Proc. IEEE Conference on Computer Vision and Pattern Recognition*, vol. 2, pp. 60–65, 2005.
- [3] S. Paris, P. Kornprobst, J. Tumblin, and F. Durand, "Bilateral filtering: Theory and Applications," *Foundations and Trends® in Computer Graphics and Vision*, vol. 4, no. 1, pp. 1–73, 2009.
- [4] P. Milanfar, "A tour of modern image filtering: New insights and methods, both practical and theoretical," *IEEE Signal Processing Magazine*, vol. 30, no. 1, pp. 106–128, 2013.
- [5] F. Durand and J. Dorsey, "Fast bilateral filtering for the display of high-dynamic-range images," *ACM Transactions on Graphics*, vol. 21, no. 3, pp. 257–266, 2002.
- [6] S. Paris and F. Durand, "A fast approximation of the bilateral filter using a signal processing approach," *Proc. European Conference on Computer Vision*, pp. 568–580, 2006.
- [7] J. Chen, S. Paris, and F. Durand, "Real-time edge-aware image processing with the bilateral grid," *ACM Transactions on Graphics*, vol. 26, no. 3, p. 103, 2007.
- [8] F. Porikli, "Constant time O(1) bilateral filtering," *Proc. IEEE Conference on Computer Vision and Pattern Recognition*, pp. 1–8, 2008.
- [9] Q. Yang, K. H. Tan, and N. Ahuja, "Real-time O(1) bilateral filtering," *Proc. IEEE Conference on Computer Vision and Pattern Recognition*, pp. 557–564, 2009.
- [10] K. N. Chaudhury, D. Sage, and M. Unser, "Fast O(1) bilateral filtering using trigonometric range kernels," *IEEE Transactions on Image Processing*, vol. 20, no. 12, pp. 3376–3382, 2011.
- [11] K. Sugimoto and S. I. Kamata, "Compressive bilateral filtering," *IEEE Transactions on Image Processing*, vol. 24, no. 11, pp. 3357–3369, 2015.
- [12] Q. Yang, N. Ahuja, and K.-H. Tan, "Constant time median and bilateral filtering," *International Journal of Computer Vision*, vol. 112, no. 3, pp. 307–318, 2015.
- [13] K. N. Chaudhury and S. D. Dabhade, "Fast and provably accurate bilateral filtering," *IEEE Transactions on Image Processing*, vol. 25, no. 6, pp. 2519–2528, 2016.
- [14] S. Ghosh and K. N. Chaudhury, "On fast bilateral filtering using Fourier kernels," *IEEE Signal Processing Letters*, vol. 23, no. 5, pp. 570–573, 2016.
- [15] K. Sugimoto, T. Breckon, and S. I. Kamata, "Constant-time bilateral filter using spectral decomposition," *Proc. IEEE International Conference on Image Processing*, pp. 3319–3323, 2016.
- [16] P. Nair, A. Popli, and K. N. Chaudhury, "A fast approximation of the bilateral filter using the discrete Fourier transform," *Image Processing On Line*, vol. 7, pp. 115–130, 2017.
- [17] G. Papari, N. Idowu, and T. Varslot, "Fast bilateral filtering for denoising large 3D images," *IEEE Transactions on Image Processing*, vol. 26, no. 1, pp. 251–261, 2017.
- [18] A. Adams, N. Gelfand, J. Dolson, and M. Levoy, "Gaussian KD-trees for fast high-dimensional filtering," *ACM Transactions on Graphics*, vol. 28, no. 3, p. 21, 2009.
- [19] A. Adams, J. Baek, and M. A. Davis, "Fast high-dimensional filtering using the permutohedral lattice," *Computer Graphics Forum*, vol. 29, no. 2, pp. 753–762, 2010.
- [20] E. S. Gastal and M. M. Oliveira, "Adaptive manifolds for real-time high-dimensional filtering," *ACM Transactions on Graphics*, vol. 31, no. 4, pp. 33:1–33:13, 2012.
- [21] M. G. Mozerov and J. Van De Weijer, "Global color sparseness and a local statistics prior for fast bilateral filtering," *IEEE Transactions on Image Processing*, vol. 24, no. 12, pp. 5842–5853, 2015.
- [22] P. Nair and K. N. Chaudhury, "Fast high-dimensional filtering using clustering," *Proc. IEEE International Conference on Image Processing*, pp. 240–244, 2017.
- [23] M. Mahmoudi and G. Sapiro, "Fast image and video denoising via nonlocal means of similar neighborhoods," *IEEE Signal Processing Letters*, vol. 12, no. 12, pp. 839–842, 2005.
- [24] J. Wang, Y. Guo, Y. Ying, Y. Liu, and Q. Peng, "Fast non-local algorithm for image denoising," *Proc. IEEE International Conference on Image Processing*, pp. 1429–1432, 2006.
- [25] J. Darbon, A. Cunha, T. F. Chan, S. Osher, and G. J. Jensen, "Fast nonlocal filtering applied to electron cryomicroscopy," *Proc. IEEE International Symposium on Biomedical Imaging*, pp. 1331–1334, 2008.
- [26] S. Ghosh and K. N. Chaudhury, "Fast separable non-local means," *Journal of Electronic Imaging*, vol. 25, no. 2, p. 023026, 2016.
- [27] —, "Fast bilateral filtering of vector-valued images," *Proc. IEEE International Conference on Image Processing*, pp. 1823–1827, 2016.
- [28] W.-C. Tu, Y.-A. Lai, and S.-Y. Chien, "Constant time bilateral filtering for color images," *Proc. IEEE International Conference on Image Processing*, pp. 3309–3313, 2016.
- [29] K. Sugimoto, N. Fukushima, and S. I. Kamata, "Fast bilateral filter for multichannel images via soft-assignment coding," *Proc. Signal and Information Processing Association Annual Summit and Conference*, pp. 1–4, 2016.
- [30] C. Karam and K. Hirakawa, "Monte-Carlo acceleration of bilateral filter and non-local means," *IEEE Transactions on Image Processing*, vol. 27, no. 3, pp. 1462–1474, 2018.
- [31] H. Talebi and P. Milanfar, "Global image denoising," *IEEE Transactions on Image Processing*, vol. 23, no. 2, pp. 755–768, 2014.
- [32] —, "Nonlocal image editing," *IEEE Transactions on Image Processing*, vol. 23, no. 10, pp. 4460–4473, 2014.
- [33] —, "Asymptotic performance of global denoising," *SIAM Journal on Imaging Sciences*, vol. 9, no. 2, pp. 665–683, 2016.
- [34] C. Williams and M. Seeger, "Using the Nyström method to speed up kernel machines," *Proc. Neural Information Processing Systems*, pp. 682–688, 2001.
- [35] C. Fowlkes, S. Belongie, F. Chung, and J. Malik, "Spectral grouping using the Nyström method," *IEEE Transactions on Pattern Analysis and Machine Intelligence*, vol. 26, no. 2, pp. 214–225, 2004.
- [36] K. Zhang, I. W. Tsang, and J. T. Kwok, "Improved Nyström low-rank approximation and error analysis," *Proc. International Conference on Machine Learning*, pp. 1232–1239, 2008.
- [37] I. T. Young and L. J. Van Vliet, "Recursive implementation of the gaussian filter," *Signal Processing*, vol. 44, no. 2, pp. 139–151, 1995.
- [38] K. Sugimoto and S. I. Kamata, "Fast gaussian filter with second-order shift property of DCT-5," *Proc. IEEE International Conference on Image Processing*, pp. 514–518, 2013.
- [39] E. J. Nyström, "Über die praktische auflösung von integralgleichungen mit anwendungen auf randwertaufgaben," *Acta Mathematica*, vol. 54, no. 1, pp. 185–204, 1930.
- [40] C. T. Baker, "The numerical treatment of integral equations," *Clarendon Press*, 1977.
- [41] V. Y. Pan and Z. Q. Chen, "The complexity of the matrix eigenproblem," *Proc. ACM Symposium on Theory of Computing*, pp. 507–516, 1999.
- [42] R. Deriche, "Recursively implementing the gaussian and its derivatives," *Research Report*, no. RR-1893, 1993.
- [43] "Matlab code." [Online]. Available: <https://github.com/pravin1390/FastHDNyström>
- [44] P.-N. Tan, M. Steinbach, and V. Kumar, *Introduction to Data Mining*. Addison-Wesley Longman Publishing Co., Inc., 2005.
- [45] T. Tasdizen, "Principal neighborhood dictionaries for nonlocal means image denoising," *IEEE Transactions on Image Processing*, vol. 18, no. 12, pp. 2649–2660, 2009.
- [46] "BM3D image database." [Online]. Available: <http://r0k.us/graphics/kodak/index.html>
- [47] "Hyperspectral image database." [Online]. Available: <http://lesun.weebly.com/hyperspectral-data-set.html>
- [48] F. Fan, Y. Ma, C. Li, X. Mei, J. Huang, and J. Ma, "Hyperspectral image denoising with superpixel segmentation and low-rank representation," *Information Sciences*, vol. 397, pp. 48–68, 2017.
- [49] Y.-Q. Zhao and J. Yang, "Hyperspectral image denoising via sparse representation and low-rank constraint," *IEEE Transactions on Geoscience and Remote Sensing*, vol. 53, no. 1, pp. 296–308, 2015.
- [50] Z. Wang, A. C. Bovik, H. R. Sheikh, and E. P. Simoncelli, "Image quality assessment: from error visibility to structural similarity," *IEEE Transactions on Image Processing*, vol. 13, no. 4, pp. 600–612, 2004.
- [51] K. Dabov, A. Foi, V. Katkovnik, and K. Egiazarian, "Image denoising with block-matching and 3D filtering," *Proc. SPIE Electronic Imaging*, vol. 6064, no. 30, pp. 1–12, 2006.